Eur. Phys. J. C 48, 3–13 (2006)
Digital Object Identifier (DOI) 10.1140/epjc/s2006-02625-4

THE EUROPEAN PHYSICAL JOURNAL C

Measurement of the strong coupling α_S from the four-jet rate in e^+e^- annihilation using JADE data

J. Schieck[1,a], S. Bethke[1], O. Biebel[2], S. Kluth[1], P.A.M. Fernández[3], C. Pahl[1], The JADE Collaboration[b]

[1] Max-Planck-Institut für Physik, Föhringer Ring 6, 80805 München, Germany
[2] Ludwig-Maximilians-Universität München, Am Coulombwall 1, 85748 Garching, Germany
[3] Lawrence Berkeley National Laboratory, 1 Cyclotron Rd., Berkeley, 94720, USA

Received: 30 May 2006 /
Published online: 19 September 2006 –

Abstract. Data from e^+e^- annihilation into hadrons collected by the JADE experiment at centre-of-mass energies between 14 GeV and 44 GeV are used to study the four-jet event production rate as a function of the Durham jet algorithm's resolution parameter $y_{\rm cut}$. The four-jet rate is compared to QCD next-to-leading order calculations including resummation of large logarithms in the next-to-leading logarithmic approximation. The strong coupling measured from the four-jet rate is

$$\alpha_{\rm S}\left(M_{\rm Z^0}\right) = 0.1159 \pm 0.0004(\text{stat.}) \pm 0.0012(\text{exp.}) \pm 0.0024(\text{had.}) \pm 0.0007(\text{theo.})$$

in agreement with the world average.

1 Introduction

The annihilation of electrons and positrons into hadrons allows precise tests of Quantum Chromodynamics (QCD). Many observables have been devised which provide a convenient way of characterizing the main features of such events. Multijet event rates are predicted in perturbation theory as functions of the jet-resolution parameter, with one free parameter, the strong coupling $\alpha_{\rm S}$. Events with four quarks in the final state, $q\bar{q}q\bar{q}$, or two quarks and two gluons, $q\bar{q}gg$, may lead to events with four-jet structure. In leading order perturbation theory, the rate of four-jet events in e^+e^-annihilation is predicted to be proportional to $\alpha_{\rm S}^2$. The strong coupling can be measured by determining the four-jet event production rate and fitting the theoretical prediction to the data.

Calculations beyond leading order are made possible by theoretical progress achieved during the last few years. For multi-jet rates as well as numerous event-shape distributions with perturbative expansions starting at $\mathcal{O}(\alpha_{\rm S})$, matched next-to-leading order (NLO) and next-to-leading logarithmic approximations (NLLA) provide a satisfactory description of the data over large kinematically allowed regions at many centre-of-mass energies [2–5].

First evidence for four-jet structure has been reported earlier by the JADE collaboration [6]. In addition multi-jet event production rates were measured and the three-jet rate was used to determine the the strong coupling $\alpha_{\rm S}$ [7–9]. The ALEPH, DELPHI and OPAL collaborations published measurements of $\alpha_{\rm S}$ based on the four-jet rate in the energy range between 91 and 209 GeV [10–12]. The same theoretical predictions as used here were employed to determine the strong coupling $\alpha_{\rm S}$.

In this analysis we use data collected by the JADE experiment in the years 1979 to 1986 at the PETRA e^+e^-collider at DESY at six centre-of-mass energies spanning the range of 14–44 GeV.

2 Observable

Jet algorithms are applied to cluster the large number of particles of a hadronic event into a small number of jets, reflecting the parton structure of the event. For this analysis we use the Durham scheme [2]. Defining each particle initially to be a proto-jet, a resolution variable y_{ij} is calculated for each pair of proto-jets i and j:

$$y_{ij} = \frac{2\min\left(E_i^2, E_j^2\right)}{E_{\rm vis}^2}\left(1 - \cos\theta_{ij}\right) , \qquad (1)$$

where E_i and E_j are the energies of jets i and j, $\cos\theta_{ij}$ is the cosine of the angle between them and $E_{\rm vis}$ is the sum of the energies of the detected particles in the event (or the partons in a theoretical calculation). If the smallest value of y_{ij} is less than a predefined value $y_{\rm cut}$, the pair is replaced by a new proto-jet with four-momentum $p_k^\mu = p_i^\mu + p_j^\mu$, and the clustering starts again. Clustering ends when

[a] e-mail: schieck@mppmu.mpg.de
[b] See [1] for the full list of authors

the smallest value of y_{ij} is larger than $y_{\rm cut}$, and the remaining proto-jets are accepted and counted as finally selected jets.

The next-to-leading order QCD calculation predicts the four-jet rate R_4, which is the fraction of four-jet events, as a function of α_S. It can be written in the following way [5]:

$$R_4(y_{\rm cut}) = \frac{\sigma_{\text{4-jet}}(y_{\rm cut})}{\sigma_{\rm tot}} = \eta^2 B_4(y_{\rm cut}) + \eta^3 \left[C_4(y_{\rm cut}) + 3/2(\beta_0 \log x_\mu - 1)\, B_4(y_{\rm cut})\right], \quad (2)$$

where $\sigma_{\text{4-jet}}(y_{\rm cut})$ is the cross-section for the production of hadronic events with four jets at fixed $y_{\rm cut}$, $\sigma_{\rm tot}$ the total hadronic cross-section, $\eta = \alpha_S\ C_F/2\pi$ with $C_F = 4/3$ the colour factor from the SU(3) symmetry group, $x_\mu = \mu/\sqrt{s}$ with μ being the renormalization scale, $\sqrt{s}$ the centre-of-mass energy, and $\beta_0 = (11 - 2n_f/3)$ with n_f the number of active flavours[1]. The coefficients B_4 and C_4 are obtained by integrating the massless matrix elements for e^+e^-annihilation into four- and five-parton final states, calculated by the program DEBRECEN 2.0 [5].

Equation (2) is used to predict the four-jet rate as a function of $y_{\rm cut}$. The fixed-order perturbative prediction is not reliable for small values of $y_{\rm cut}$, due to terms of the form $\alpha_S^n \ln^m(y_{\rm cut})$ which enhance the higher order corrections. An all-order resummation of such terms in the NLLA is possible for the Durham clustering algorithm [2]. The NLLA calculation is combined with the NLO-prediction using the so-called modified R-matching scheme [13]. In the modified R-matching scheme the terms proportional to η^2 and η^3 are removed from the NLLA prediction $R^{\rm NLLA}$ and the difference is then added to the NLO calculation $R^{\rm NLO}$ with the result:

$$R^{\text{R-match}} = R^{\rm NLLA} + [\eta^2(B_4 - B^{\rm NLLA}) + \eta^3(C_4 - C^{\rm NLLA} - 3/2(B_4 - B^{\rm NLLA}))], \quad (3)$$

where $B^{\rm NLLA}$ and $C^{\rm NLLA}$ are the coefficients of the expansion of $R^{\rm NLLA}$ as in (2) and the x_μ term and $y_{\rm cut}$ dependence have been suppressed for clarity.

3 Analysis procedure

3.1 The JADE detector

A detailed description of the JADE detector can be found in [1]. This analysis relies mainly on the reconstruction of charged particle trajectories and on the measurement of energy deposited in the electromagnetic calorimeter. Tracking of charged particles was performed with the central tracking detector, which was positioned in a solenoidal magnet providing an axial magnetic field of 0.48 T. The central detector contained a large volume jet chamber. Later a vertex chamber close to the interaction point and surrounding z-chambers to measure the z-coordinate [2] were added. Most of the tracking information is obtained from the jet chamber, which provides up to 48 measured space points per track, and good tracking efficiency in the region $|\cos\theta| < 0.97$. Electromagnetic showers are measured by the lead glass calorimeter surrounding the magnet coil, separated into a barrel ($|\cos\theta| < 0.839$) and two end-cap ($0.86 < |\cos\theta| < 0.97$) sections. The electromagnetic calorimeter consisted of 2520 lead glass blocks with a depth of 12.5 radiation lengths in the barrel (since 1983 increased to 15.7 in the middle 20% of the barrel) and 192 lead glass blocks with 9.6 radiation lengths in the end-caps.

[1] In this analysis the number of active flavours is set to five.

Table 1. The average centre-of-mass energy, the energy range, the year of data taking and the integrated luminosity for each data sample, together with the numbers of selected data events

average energy in GeV	energy range in GeV	year	luminosity (pb^{-1})	selected events
14.0	13.0–15.0	1981	1.46	1783
22.0	21.0–23.0	1981	2.41	1403
34.6	33.8–36.0	1981–1982	61.7	14313
35.0	34.0–36.0	1986	92.3	20876
38.3	37.3–39.3	1985	8.28	1585
43.8	43.4–46.4	1984–1985	28.8	4374

3.2 Data samples

The data used in this analysis were collected by JADE between 1979 and 1986 and correspond to a total integrated luminosity of 195 pb^{-1}. The breakdown of the data samples, average centre-of-mass energy, energy range, data taking period, collected integrated luminosities and the size of the data samples after selection of hadronic events are given in Table 1. The data samples are chosen following previous analyses, e.g. [1, 9, 14–16][3].

3.3 Monte Carlo samples

Samples of Monte Carlo simulated events are used to correct the data for experimental acceptance, resolution and backgrounds. The process $e^+e^- \to$ hadrons is simulated using PYTHIA 5.7 [17]. Corresponding samples using HERWIG 5.9 [18] are used for systematic checks. The Monte Carlo samples generated at each energy point are

[2] In the JADE right-handed coordinate system the $+x$ axis points towards the centre of the PETRA ring, the y axis pointed upwards and the z axis points in the direction of the positron beam. The polar angle θ and the azimuthal angle ϕ are defined with respect to z and x, respectively, while r is the distance from the z-axis.

[3] The data are available from two versions of the reconstruction software from 9/87 and from 5/88. We use the set from 5/88 as the default version and consider differences between the results as an experimental systematic uncertainty.

processed through a full simulation of the JADE detector [19–22], and reconstructed in essentially the same way as the data. In addition, for comparisons with the corrected data, and when correcting for the effects of hadronization, large samples of Monte Carlo events without detector simulation are employed, using the parton shower models PYTHIA 6.158, HERWIG 6.2 and ARIADNE 4.11 [23]. Each of these hadronization models contains a number of tunable parameters; these were adjusted by tuning to previously published OPAL data at $\sqrt{s} \sim 91\,\mathrm{GeV}$ as summarized in [24] for PYTHIA/JETSET and in [25] for HERWIG and ARIADNE. The data taken by the JADE experiment are well described by the Monte Carlo simulated events [16], with only the centre-of-mass energy changed and set to the respective value of the event.

3.4 Selection of events

The selection of events for this analysis aims to identify hadronic event candidates and to reject events with a large amount of energy emitted by initial state photon radiation (ISR). The selection of hadronic events is based on cuts on event multiplicity to remove leptonic final states and on visible energy and longitudinal momentum imbalance to remove radiative and two-photon events, $e^+e^- \to e^+e^-+$ hadrons. The cuts are documented in [8, 26, 27] and summarized in a previous publication [14]:

Standard criteria are used to select good tracks and clusters of energy deposits in the calorimeter for subsequent analysis. For charged particle tracks the pion mass was assigned while for clusters zero mass particles are assumed. Charged particle tracks are required to have at least 20 hits in $r-\phi$ and at least 12 hits in $r-z$ in the jet chamber. The total momentum is required to be at least 100 MeV. Furthermore, the point of closest approach of the track to the collision axis is required to be less than 5 cm from the nominal collision point in the $x-y$ plane and less than 35 cm in the $z-$direction.

In order to mitigate the effects of double counting of energy from tracks and calorimeter clusters a standard algorithm is adopted which associates charged particles with calorimeter clusters, and subtracts the estimated contribution of the charged particles from the cluster energy. Clusters in the electromagnetic calorimeter are required to have an energy exceeding 0.15 GeV after the subtraction of the expected energy deposit of associated tracks. From all accepted tracks and clusters the visible energy $E_{\mathrm{vis}} = \sum_i E_i$, momentum balance $p_{\mathrm{bal}} = |\sum_i p_{z,i}|/E_{\mathrm{vis}}$ and missing momentum $p_{\mathrm{miss}} = |\sum_i p_i|$ are calculated.

Hadronic event candidates are required to pass the following selection criteria:

- The total energy deposited in the electromagnetic calorimeter has to exceed 1.2 GeV (0.2 GeV) for $\sqrt{s} <$ 16 GeV, 2.0 GeV (0.4 GeV) for $16 < \sqrt{s} < 24$ GeV and 3.0 GeV (0.4 GeV) for $\sqrt{s} > 24$ GeV in the barrel (each endcap) of the detector.
- Events with exactly four tracks with configurations where three tracks are in one hemisphere and one track is in the opposite hemisphere are rejected.
- At least three tracks have to have more than 24 hits in $r-\phi$ and a momentum in the $x-y$ plane larger than 500 MeV; these tracks are called long tracks.
- The visible energy has to fulfill $E_{\mathrm{vis}}/\sqrt{s} > 0.5$.
- The momentum balance has to fulfill $p_{\mathrm{bal}} < 0.4$.
- The missing momentum has to fulfill $p_{\mathrm{miss}}/\sqrt{s} < 0.3$.
- The z-coordinate of the reconstructed event vertex has to lie within 15 cm of the interaction point.
- The polar angle of the event thrust axis [28] is required to satisfy $|\cos(\theta_{\mathrm{T}})| < 0.8$ in order that the events be well contained within the detector acceptance.
- The number of good charged particle tracks is required to be greater than three reducing $\tau^+\tau^-$ and two-photon backgrounds to a negligible level.

The numbers of selected events for each centre-of-mass energy are shown in Table 1.

3.5 Corrections to the data

All selected tracks and electromagnetic calorimeter clusters are used in the evaluation of the four-jet rate. The four-jet rate distribution as a function of the jet resolution y_{cut} after all selection cuts applied is called the detector-level distribution.

In this analysis events from the process $e^+e^- \to b\bar{b}$ systematically bias our results, since especially at low centre-of-mass energies the large mass of the b quarks and of the subsequently produced and decaying B hadrons will influence the four-jet rate distribution [10–12]. The QCD predictions are calculated for massless quarks and thus we choose to correct our data for the presence of $b\bar{b}$ events. About 1/11 of all $q\bar{q}$ events are $b\bar{b}$ events. The expected number of $b\bar{b}$ background events η_i is subtracted from the observed number of data events N_i at each y_{cut} bin i. The effects of detector acceptance and resolution and of residual ISR are then accounted for by a multiplicative correction procedure.

Two distributions are formed from Monte Carlo simulated signal events; the first, at the detector-level, treats the Monte Carlo events identically to the data, while the second, at the hadron-level, is computed using the true four-momenta of the stable particles[4], and is restricted to events where $\sqrt{s'}$, the centre-of-mass energy reduced due to ISR, satisfies $\sqrt{s} - \sqrt{s'} < 0.15\,\mathrm{GeV}$. The ratio of the Monte Carlo distribution taken at the hadron-level to the distribution taken at the detector-level for each y_{cut} bin i, C_i^{detector}, is used as a correction factor for the data. This finally yields the corrected number of four jet events at y_{cut} bin i, $\tilde{N}_i = C_i^{\mathrm{detector}} \cdot (N_i - \eta_i)$. The hadron-level distribution is then normalized at each y_{cut} bin i by calculating $R_{4,i} = \tilde{N}_i/N$, where the N is the corrected number of events selected at hadron-level. We observe some disagreement between the detector corrections calculated using PYTHIA or HERWIG at low centre-of-mass energies while at larger $\sqrt{s}$ the correction factors agree well within

[4] All charged and neutral particles with a lifetime longer than 3×10^{-10} s are treated as stable.

the regions chosen for comparison with the theory predictions. The difference in detector corrections is evaluated as an experimental systematic uncertainty. The numerical results of the four-jet rate at hadron-level at the different energy points are summarized in Tables 5 and 6.

4 Systematic uncertainties

Several sources of possible systematic uncertainties are studied. Uncertainties originating from massless quark calculations are not considered, since contributions to the four-jet rate from B hadrons are subtracted at detector-level. For each variation of parameters the difference of the resulting value of α_S with respect to the default value is taken as a systematic uncertainty. The default value of α_S is determined with the standard event selection and the correction procedure using PYTHIA. The systematic uncertainty is taken to be symmetric around the default value of α_S.

4.1 Experimental uncertainties

Contributions to the experimental uncertainties are estimated by repeating the analysis with varied cuts or procedures. For each systematic variation the value of α_S is determined and then compared to the result of the standard analysis (default value).

1. In the standard analysis the reconstruction software from 5/88 is used. As a variation a different reconstruction software from 9/87 is used.
2. In the default method the estimated minimum ionizing energy from tracks associated with electromagnetic calorimeter clusters is subtracted from the cluster energies. As a variation all accepted tracks and all uncorrected electromagnetic clusters are used.
3. The thrust axis is required to satisfy $|\cos(\theta_T)| < 0.7$. With this more stringent cut events are restricted to the barrel region of the detector, which provides better measurements of tracks and clusters compared to the endcap regions.
4. Instead of using PYTHIA for the correction of detector effects as described in Sect. 3.5, events generated with HERWIG are used.
5. The requirement on missing momentum is dropped or tightened to $p_{\mathrm{miss}}/\sqrt{s} < 0.25$. The larger deviation from the default value is taken as a systematic uncertainty.
6. The requirement on the momentum balance is dropped or tightened to $p_{\mathrm{bal}} < 0.3$. The larger deviation from the default value is taken as a systematic uncertainty.
7. The requirement on the number of long tracks is tightened to $N_{\mathrm{long}} \geq 4$.
8. The requirement on the visible energy is varied to $E_{\mathrm{vis}}/\sqrt{s} > 0.45$ and $E_{\mathrm{vis}}/\sqrt{s} > 0.55$. The larger deviation from the default value is taken as a systematic uncertainty.
9. The fit range is changed. Two different cases are considered. First the fit range is reduced by one data point at each edge of the standard fit range. Second the fit range is extended by one data point at each edge of the standard fit range. The larger deviation from the default fit is taken as a systematic uncertainty. In order to take statistical fluctuations into account, the deviation is calculated using the average deviation of a fit applied to 50 Monte Carlo samples.
10. The amount of subtracted $b\bar{b}$ background is varied by $\pm 5\%$ of its nominal value of about 1/11 to cover uncertainties in the estimation of the background fraction in the data. The larger deviation from the default value is taken as the systematic uncertainty.

All contributions listed above are added in quadrature and the result is quoted as the experimental systematic uncertainty. The dominating effects are the use of the different data versions and the different correction for detector effects.

4.2 Hadronization

The uncertainties associated with the hadronization correction (see Sect. 5.2) are assessed by using HERWIG and ARIADNE instead of the default hadronization correction using PYTHIA. The larger change in α_S resulting from these alternatives is taken to define the symmetric hadronization systematic uncertainty.

4.3 Theoretical uncertainties

The theoretical uncertainty, associated with missing higher order terms in the theoretical prediction, is assessed by varying the renormalization scale factor x_μ. The predictions of a complete QCD calculation would be independent of x_μ, but a finite-order calculation such as that used here retains some dependence on x_μ. The renormalization scale factor x_μ is set to 0.5 and two. The larger deviation from the default value of α_S is taken as systematic uncertainty.

5 Results

5.1 Four-Jet rate distributions

The four-jet rates for the six centre-of-mass energy points after subtraction of $b\bar{b}$ background and correction for detector effects are shown in Fig. 1. Superimposed are the distributions predicted by the PYTHIA, HERWIG and ARIADNE Monte Carlo models. Towards large y_{cut} values (right to the maximum of the distribution) the decrease of the four-jet rate corresponds to the migration and classification to three- and two-jet events. Towards smaller y_{cut} values (left to the maximum of the distribution) the decrease corresponds to the migration and classification to five or more jet events, i.e. towards the higher order QCD and non-perturbative or hadronization region. In order to make a more clear comparison between data and models, the inserts in the upper right corner show the differences between data and each model, divided by the combined

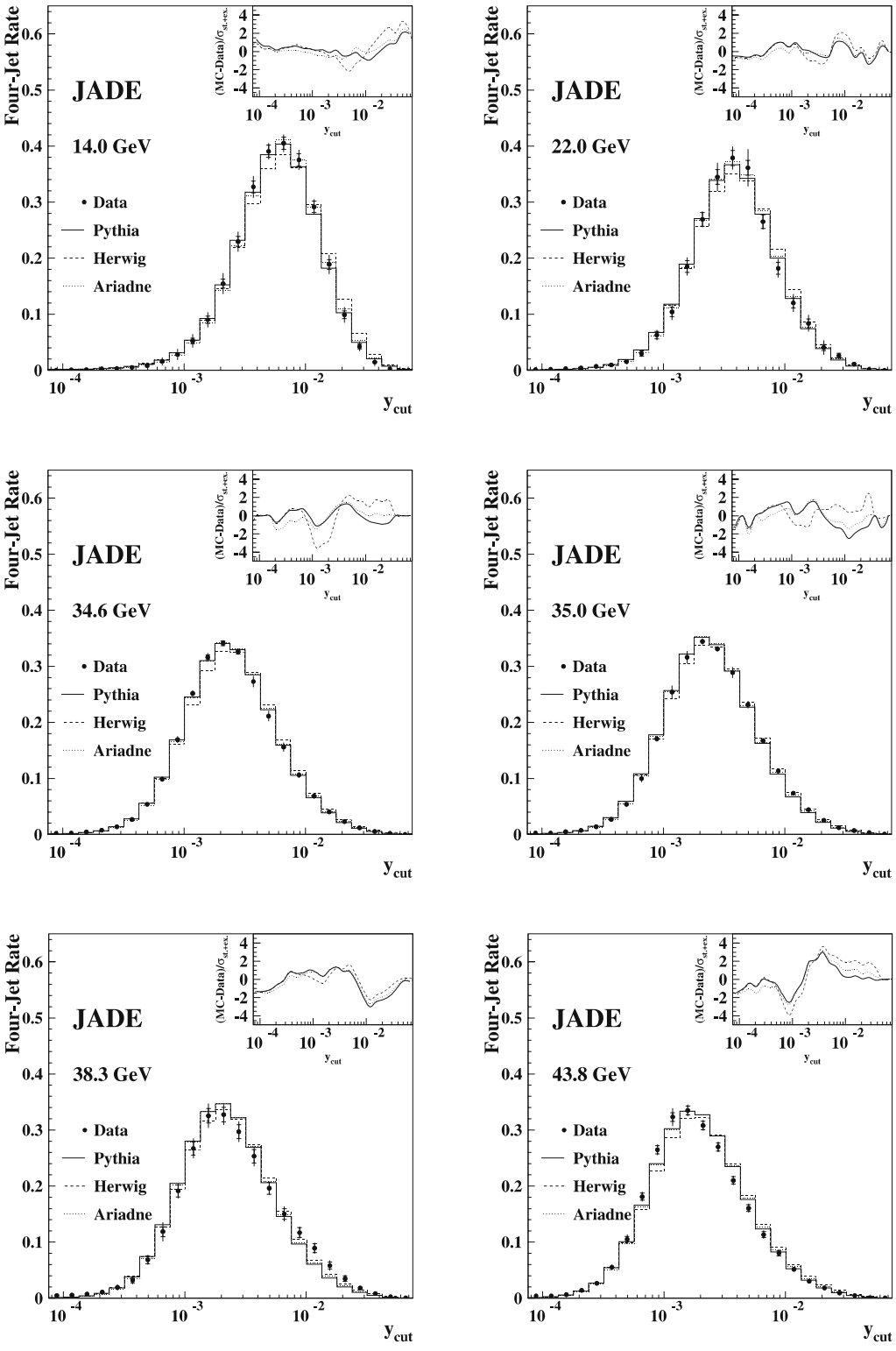

Fig. 1. The figures show the four-jet rate distribution corrected for detector effects at hadron-level as a function of the $y_{\rm cut}$ resolution parameter obtained with the Durham algorithm. The four-jet rate at four average centre-of-mass energies are shown for $\sqrt{s} =$ 14 to 43.8 GeV in comparison with predictions based on PYTHIA, HERWIG and ARIADNE Monte Carlo events. The expected $\mathrm{b\bar{b}}$ background is subtracted from the data. The error bars show the statistical (inner part) and the experimental and statistical uncertainties added in quadrature. The panel in each upper right corner shows the differences between data and Monte Carlo, divided by the quadratic sum of the statistical and experimental error. At points with no data events, the difference is set to zero

statistical and experimental error at that point. The sum of squares of these differences would, in the absence of point-to-point correlations, represent a χ^2 between data and the model. However, since correlations are present, such χ^2 values should be regarded only as a rough indication of the agreement between data and the models. The three models are seen to describe the data well.

5.2 Determination of α_S

Our measurement of the strong coupling α_S is based on χ^2 fits of QCD predictions to the corrected four-jet rate distribution, i.e. the data shown in Fig. 1. The theoretical predictions of the four-jet rate using the combined $\mathcal{O}(\alpha_S^3)$+NLLA calculation as described in Sect. 2 provide

distributions at the parton-level. In the Monte Carlo simulation the parton-level distributions are obtained from the partons after the parton shower has stopped, just before the hadronization. In order to confront the theory with the hadron-level data, it is necessary to correct for hadronization effects. This is done by calculating the distributions at both the hadron and the parton-level using PYTHIA and, as a cross-check, with the HERWIG and ARIADNE models. The theoretical prediction is then multiplied by the ratio of the hadron- and parton-level distributions.

The differences between the models are considered as a systematic uncertainty.

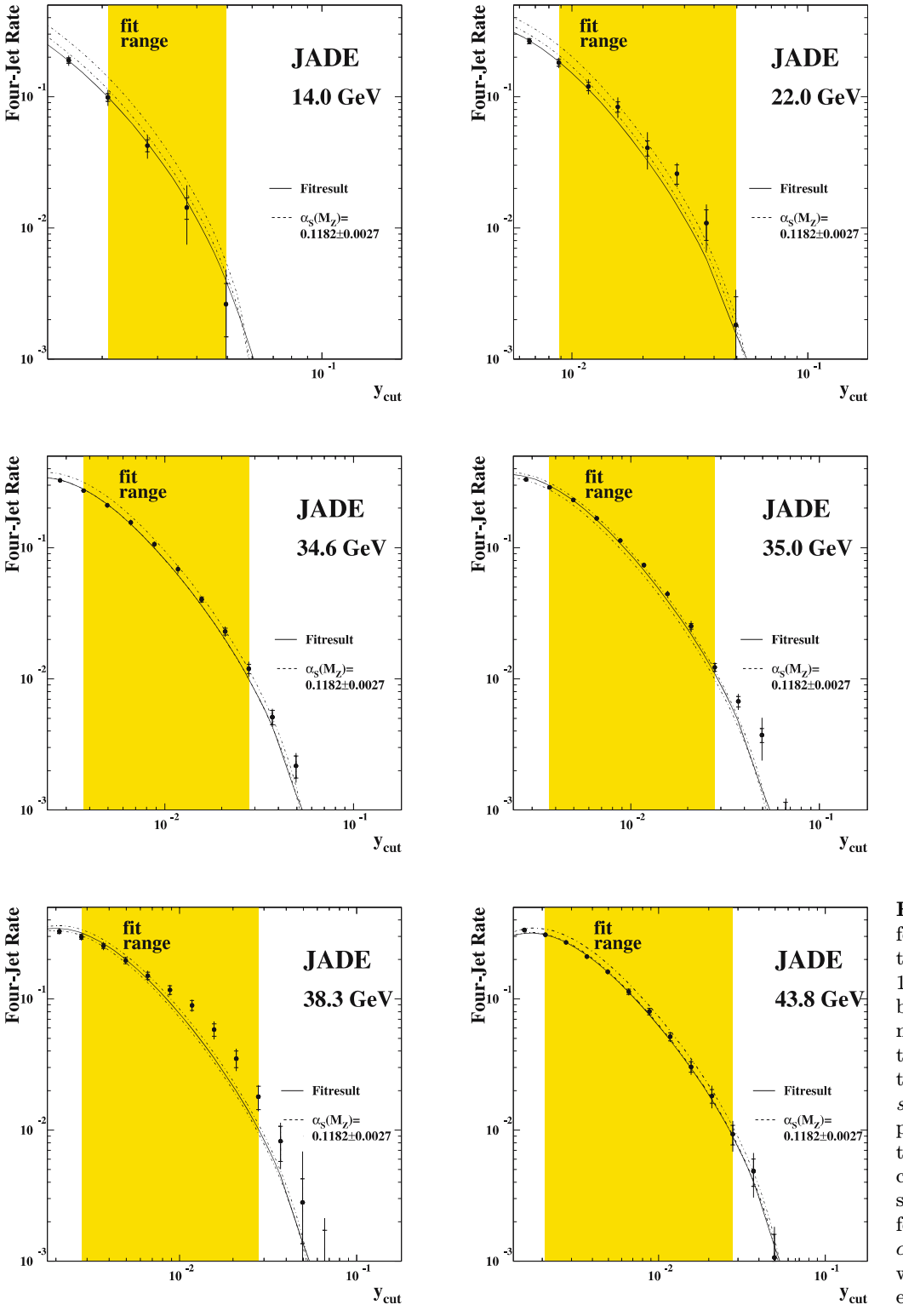

Fig. 2. The plots show the four-jet rate distributions at the hadron-level for $\sqrt{s}$ = 14 GeV to 43.8 GeV. The error bars show the statistical (inner part) and the experimental and statistical uncertainties added in quadrature. The *solid curve* shows the theory prediction after χ^2 minimization within the fit range indicated. The *dash-dotted lines* show the error band of the four-jet rate prediction with $\alpha_S(M_{Z^0})$ being the current world average value and its error [29]

Table 2. The value of α_S for each energy point and the statistical, experimental, hadronization and scale errors. The last column corresponds to the χ^2/d.o.f. value of the fit

$\sqrt{s}$ [GeV]	$\alpha_S(\sqrt{s})$	stat.	exp.	hadr.	scale	χ^2/d.o.f.
14.0	0.1536	0.0032	0.0064	0.0028	0.0074	1.46/3
22.0	0.1407	0.0028	0.0034	0.0021	0.0024	14.22/6
34.6	0.1346	0.0007	0.0019	0.0031	0.0011	17.20/7
35.0	0.1391	0.0006	0.0017	0.0033	0.0012	23.51/7
38.3	0.1355	0.0021	0.0042	0.0038	0.0020	19.78/8
43.8	0.1289	0.0012	0.0011	0.0038	0.0019	4.02/9

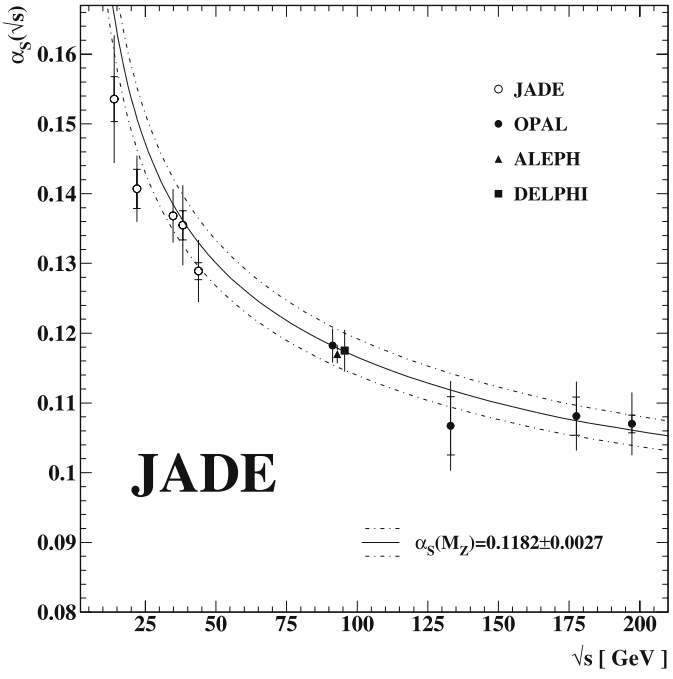

Fig. 3. The values for α_S at the various energy points. The errors show the statistical (inner part) and the total error. The *full* and *dash-dotted lines* indicate the current world average value of α_S (M_{Z^0}) [29] with error. The results at $\sqrt{s} = 34.6$ and 35 GeV have been combined for clarity. The results from the LEP experiments ALEPH [10], DELPHI [11] and OPAL [12] are shown as well

Table 4. The value of α_S and the statistical, experimental, hadronization, the renormalization scale scale factor $x_\mu^{\min}$ and the χ^2/d.o.f. value of the fit for the energy points between 22 and 43.8 GeV with α_S having the least sensitivity to the renormalization scale x_μ

$\sqrt{s}$ [GeV]	$\alpha_S(\sqrt{s})$	stat.	exp.	hadr.	$x_\mu^{\min}$	χ^2/d.o.f.
22.0	0.1391	0.0027	0.0034	0.0018	0.42	13.61/6
34.6	0.1345	0.0007	0.0019	0.0031	0.92	15.38/7
35.0	0.1391	0.0006	0.0017	0.0033	0.92	20.78/7
38.3	0.1354	0.0021	0.0042	0.0038	1.15	20.80/8
43.8	0.1288	0.0012	0.0011	0.0038	1.22	4.50/9

A χ^2-value at each energy point is calculated using the following formula:

$$\chi^2 = \sum_{i,j}^{n} \left(R_{4,i} - R(\alpha_S)_{4,i}^{\text{theo}}\right) \left(V(R_4)^{-1}\right)_{ij} \times \left(R_{4,j} - R(\alpha_S)_{4,j}^{\text{theo}}\right) , \quad (4)$$

where the indices i and j denote the y_{cut} bins in the chosen fit range and the $R(\alpha_S)_{4,i}^{\text{theo}}$ are the predicted values of the four-jet rate. The four-jet rate as a function of y_{cut} is an integrated distribution and therefore a single event can contribute to several y_{cut} bins and neighboring y_{cut} bins are correlated. The covariance matrix V_{ij} is calculated using the matrix W_{ij} determined from four-jet rate distributions calculated from Monte-Carlo at the hadron-level as follows:

$$W_{ij} = \frac{1}{n-1}\left[\sum_{k=1}^{n} x_i^k x_j^k - \frac{1}{n}\sum_{k=1}^{n} x_i^k \sum_{k=1}^{n} x_j^k\right] , \quad (5)$$

where x_i^k is the average jet rate for a given y_{cut} bin i and sample k, and n is the number of subsamples. Subsamples are built by choosing 1000 events randomly out of the set of all generated Monte Carlo events. A single event may be included in several subsamples, but the impact on the final covariance matrix is expected to be very small and, therefore, is neglected [30]. For every centre-of-mass energy point 1000 subsamples are built. The matrix W_{ij} is then used to determine the correlation matrix, $\rho_{ij} = W_{ij}/\tilde{\sigma}_i\tilde{\sigma}_j$, with $\tilde{\sigma}_i = \sqrt{W_{ii}}$. The covariance matrix $V_{ij}(R_4)$ used in the

Table 3. The value of α_S and the statistical, experimental, hadronization, renormalization scale factor x_μ^{opt}, the correlation between α_S and the renormalization scale factor and the χ^2/d.o.f. value of the fit for all energy points with the minimization performed using the optimized renormalization scheme

$\sqrt{s}$ [GeV]	$\alpha_S(\sqrt{s})$	stat.	exp.	hadr.	x_μ^{opt}	Corr.	χ^2/d.o.f.
14.0	0.1572	0.0033	0.0065	0.0031	1.49 ± 0.50	0.66	0.01/2
22.0	0.1393	0.0027	0.0033	0.0019	0.55 ± 0.31	0.28	13.38/5
34.6	0.1357	0.0007	0.0019	0.0030	0.44 ± 0.07	-0.68	4.09/6
35.0	0.1401	0.0006	0.0017	0.0031	0.46 ± 0.06	-0.67	6.04/6
38.3	0.1416	0.0024	0.0049	0.0039	0.33 ± 0.05	-0.68	10.98/7
43.8	0.1291	0.0012	0.0011	0.0037	0.87 ± 0.33	-0.44	3.90/8

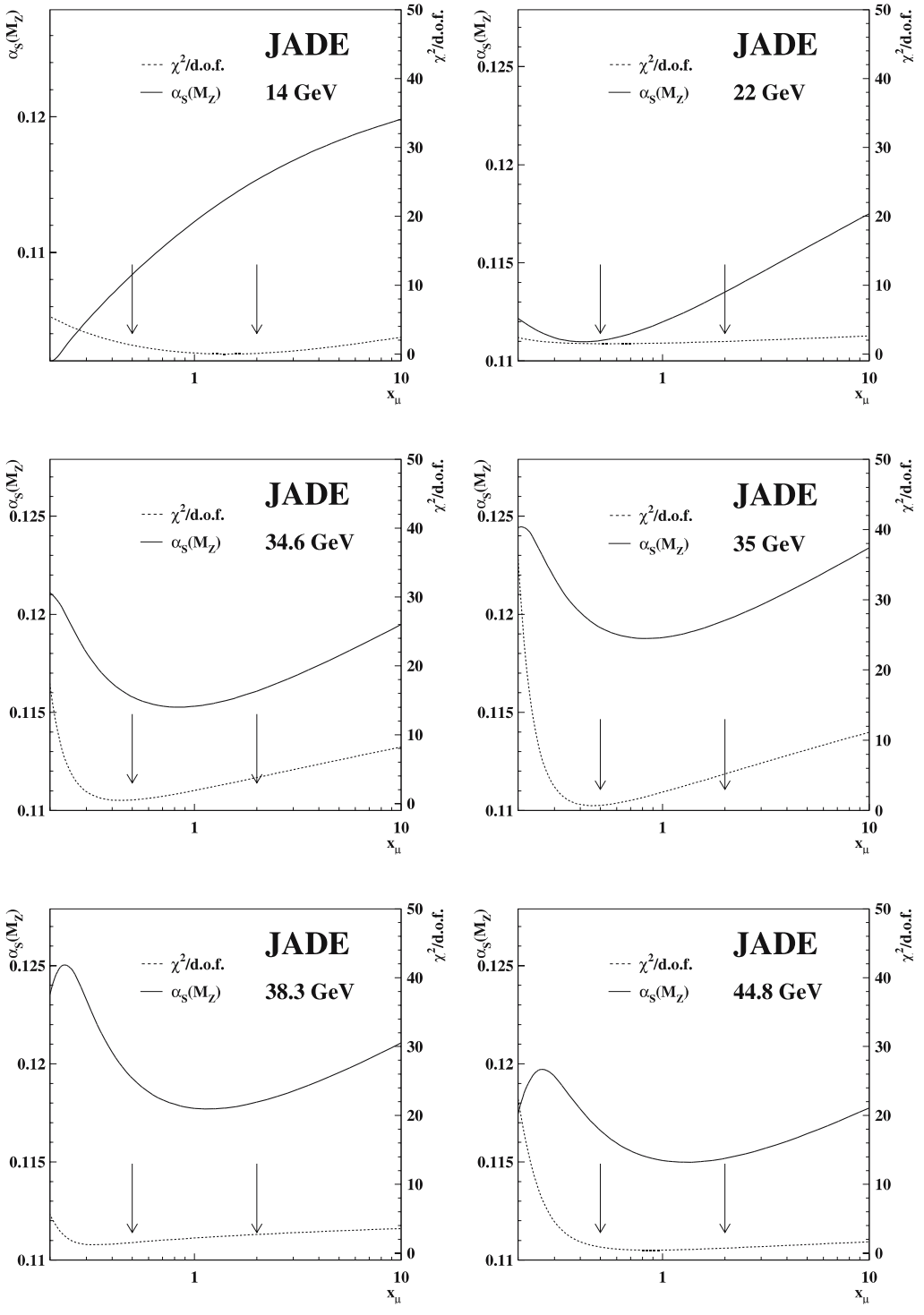

Fig. 4. The result of $\alpha_S\,(M_{Z^0})$and the χ^2/d.o.f. of the fit to the four-jet rate as a function of the renormalization scale x_μ for $\sqrt{s} = 14$ GeV to 43.8 GeV. The arrows indicate the variation of the renormalization scale factor used for the determination of the systematic uncertainties

χ^2 fit is then determined using the statistical error σ_i of the data sample at data point i and the correlation matrix $\rho_{ij} : V_{ij}(R_4) = \rho_{ij}\sigma_i\sigma_j$.

The χ^2 value is minimized with respect to α_S for each centre-of-mass energy point separately. The renormalization scale factor x_μ, as discussed in Sect. 2, is set to one.

The fit ranges are determined by requiring that the hadronization corrections be less than 50% and the detector corrections be less than 50% in the fit range. In order to exclude the non-perturbative region we require $\sqrt{s \cdot y_{\rm cut}}$ to be larger than 2 GeV. In the Durham scheme this value corresponds to the minimal transverse momentum of the pair of proto-jets with respect to each other. The fit range is $0.0209 < y_{\rm cut} < 0.0495$ for data taken at 14 GeV, $0.0088 < y_{\rm cut} < 0.0495$ for data taken at 22 GeV, $0.0037 < y_{\rm cut} < 0.0279$ for data taken at 34.6 and 35 GeV, $0.0028 < y_{\rm cut} < 0.0279$ for data taken at 38.3 GeV and $0.0021 < y_{\rm cut} < 0.0279$ for data taken at 43.8 GeV. In Fig. 2

Table 5. Hadron-level value of the four-jet fraction using the Durham algorithm at 14, 22 and 34.6 GeV. In all cases the first quoted error indicates the statistical error while the second quoted error corresponds to the total experimental uncertainty. Uncertainties consistent with zero indicate that the corresponding value is smaller than the precision shown in the table

$\log_{10}(y_{\rm cut})$	$R_4(14\,\text{GeV})$	$R_4(22\,\text{GeV})$	$R_4(34.6\,\text{GeV})$
−4.68			$0.004 \pm 0.001 \pm 0.005$
−4.55		$0.008 \pm 0.002 \pm 0.014$	$0.002 \pm 0.000 \pm 0.002$
−4.43		$0.002 \pm 0.001 \pm 0.003$	$0.002 \pm 0.000 \pm 0.002$
−4.30		$0.002 \pm 0.001 \pm 0.002$	$0.002 \pm 0.000 \pm 0.001$
−4.18		$0.002 \pm 0.001 \pm 0.001$	$0.002 \pm 0.000 \pm 0.001$
−4.05		$0.001 \pm 0.001 \pm 0.001$	$0.002 \pm 0.000 \pm 0.001$
−3.93	$0.001 \pm 0.001 \pm 0.001$	$0.002 \pm 0.001 \pm 0.000$	$0.003 \pm 0.001 \pm 0.001$
−3.81	$0.001 \pm 0.001 \pm 0.002$	$0.003 \pm 0.002 \pm 0.001$	$0.004 \pm 0.001 \pm 0.001$
−3.68	$0.003 \pm 0.001 \pm 0.003$	$0.004 \pm 0.002 \pm 0.002$	$0.008 \pm 0.001 \pm 0.001$
−3.56	$0.003 \pm 0.001 \pm 0.003$	$0.007 \pm 0.002 \pm 0.002$	$0.014 \pm 0.001 \pm 0.001$
−3.43	$0.005 \pm 0.002 \pm 0.003$	$0.009 \pm 0.003 \pm 0.002$	$0.027 \pm 0.001 \pm 0.002$
−3.31	$0.008 \pm 0.002 \pm 0.004$	$0.015 \pm 0.003 \pm 0.003$	$0.054 \pm 0.002 \pm 0.003$
−3.18	$0.016 \pm 0.003 \pm 0.006$	$0.030 \pm 0.005 \pm 0.004$	$0.099 \pm 0.003 \pm 0.004$
−3.06	$0.028 \pm 0.004 \pm 0.009$	$0.063 \pm 0.007 \pm 0.006$	$0.169 \pm 0.003 \pm 0.005$
−2.93	$0.052 \pm 0.005 \pm 0.011$	$0.104 \pm 0.008 \pm 0.012$	$0.252 \pm 0.004 \pm 0.004$
−2.81	$0.090 \pm 0.006 \pm 0.012$	$0.185 \pm 0.011 \pm 0.012$	$0.316 \pm 0.004 \pm 0.006$
−2.68	$0.155 \pm 0.008 \pm 0.017$	$0.269 \pm 0.012 \pm 0.007$	$0.341 \pm 0.004 \pm 0.003$
−2.56	$0.229 \pm 0.009 \pm 0.015$	$0.345 \pm 0.013 \pm 0.021$	$0.326 \pm 0.004 \pm 0.003$
−2.43	$0.327 \pm 0.011 \pm 0.017$	$0.379 \pm 0.013 \pm 0.016$	$0.273 \pm 0.004 \pm 0.009$
−2.31	$0.391 \pm 0.011 \pm 0.010$	$0.361 \pm 0.013 \pm 0.031$	$0.211 \pm 0.004 \pm 0.008$
−2.18	$0.405 \pm 0.011 \pm 0.011$	$0.265 \pm 0.012 \pm 0.007$	$0.156 \pm 0.003 \pm 0.007$
−2.06	$0.375 \pm 0.011 \pm 0.015$	$0.182 \pm 0.011 \pm 0.013$	$0.106 \pm 0.003 \pm 0.005$
−1.93	$0.291 \pm 0.010 \pm 0.009$	$0.120 \pm 0.009 \pm 0.013$	$0.069 \pm 0.002 \pm 0.004$
−1.80	$0.189 \pm 0.009 \pm 0.015$	$0.084 \pm 0.008 \pm 0.013$	$0.040 \pm 0.002 \pm 0.002$
−1.68	$0.099 \pm 0.007 \pm 0.012$	$0.041 \pm 0.005 \pm 0.012$	$0.023 \pm 0.001 \pm 0.002$
−1.55	$0.043 \pm 0.004 \pm 0.007$	$0.026 \pm 0.004 \pm 0.003$	$0.012 \pm 0.001 \pm 0.001$
−1.43	$0.014 \pm 0.003 \pm 0.006$	$0.011 \pm 0.003 \pm 0.003$	$0.005 \pm 0.001 \pm 0.001$
−1.30	$0.003 \pm 0.001 \pm 0.002$	$0.002 \pm 0.001 \pm 0.001$	$0.002 \pm 0.000 \pm 0.000$
−1.18	$-0.001 \pm 0.001 \pm 0.001$		

the hadron-level four-jet distributions with the fit results for the six energy points are shown together with the four-jet rate prediction with α_S being the current world average. The results of the fits are summarized in Table 2. The statistical uncertainties correspond to the uncertainty from the χ^2 minimization, while the systematic errors are determined as described in Sect. 4.

It is of interest to combine the measurements of α_S from the different centre-of-mass energy points in order to determine a single value of α_S at a common energy scale. The fit results for α_S are combined using the procedure of [31]. In brief the method is as follows. The set of α_S measurements to be combined are first evolved to a common scale, $Q = M_{Z^0}$, assuming the validity of QCD and M_{Z^0} being the mass of the Z^0 vector boson. The measurements are then combined in a weighted mean, to minimize the χ^2 between the combined value and the measurements. If the measured values evolved to $Q = M_{Z^0}$ are denoted $\alpha_{S,i}$, with covariance matrix V', the combined value, $\alpha_S(M_{Z^0})$, is given by

$$\alpha_S(M_{Z^0}) = \sum w_i \alpha_{S,i}\,, \quad \text{where } w_i = \frac{\sum_j \left(V'^{-1}\right)_{ij}}{\sum_{j,k}\left(V'^{-1}\right)_{jk}}\,, \quad (6)$$

where i and j denote the six individual results. The difficulty resides in making a reliable estimate of V' in the presence of dominant and highly correlated systematic errors. Small uncertainties in the estimation of these correlations can cause undesirable features such as negative weights. For this reason only experimental systematic errors assumed to be partially correlated between measurements contribute to the off-diagonal elements of the covariance matrix: $V'_{ij} = \min(\sigma^2_{\text{exp},i}, \sigma^2_{\text{exp},j})$. All error contributions (statistical, experimental, hadronization and scale uncertainty) contribute to the diagonal elements only. The hadronization and scale uncertainties are computed by combining the α_S values obtained with the alternative hadronization models, and from the upper and lower theoretical errors, using the weights derived from the covariance matrix V'.

The fit result from the 14 GeV data has large experimental and theoretical uncertainties. We therefore choose to not include this result in the combination. The combination using all results for $\sqrt{s} \geq 22$ GeV is

$$\begin{aligned}\alpha_S(M_{Z^0}) = 0.1159 &\pm 0.0004(\text{stat.}) \pm 0.0012(\text{exp.}) \\ &\pm 0.0024(\text{had.}) \pm 0.0007(\text{theo.})\,, \end{aligned} \quad (7)$$

consistent with the world average value of $\alpha_S(M_{Z^0}) = 0.1182 \pm 0.0027$ [29]. The weights w_i as described in (6) are 0.15 for 22 GeV, 0.29 for 34.6 GeV, 0.29 for 35 GeV,

Table 6. Hadron-level value of the four-jet fraction using the Durham algorithm at 35, 38.3 and 43.8 GeV. In all cases the first quoted error indicates the statistical error while the second quoted error corresponds to the total experimental uncertainty. Uncertainties consistent with zero indicate that the corresponding value is smaller than the precision shown in the table

$\log_{10}(y_{\rm cut})$	$R_4(35\,\text{GeV})$	$R_4(38.3\,\text{GeV})$	$R_4(43.8\,\text{GeV})$
−4.80	$0.001 \pm 0.000 \pm 0.001$		
−4.68	$0.003 \pm 0.000 \pm 0.004$	$0.001 \pm 0.001 \pm 0.001$	
−4.55	$0.002 \pm 0.000 \pm 0.002$	$0.001 \pm 0.001 \pm 0.001$	$0.011 \pm 0.002 \pm 0.014$
−4.43	$0.002 \pm 0.000 \pm 0.002$	$0.004 \pm 0.002 \pm 0.004$	$0.004 \pm 0.001 \pm 0.004$
−4.30	$0.002 \pm 0.000 \pm 0.002$	$0.005 \pm 0.002 \pm 0.004$	$0.004 \pm 0.001 \pm 0.004$
−4.18	$0.003 \pm 0.000 \pm 0.002$	$0.004 \pm 0.002 \pm 0.002$	$0.004 \pm 0.001 \pm 0.003$
−4.05	$0.002 \pm 0.000 \pm 0.001$	$0.005 \pm 0.002 \pm 0.002$	$0.004 \pm 0.001 \pm 0.002$
−3.93	$0.003 \pm 0.000 \pm 0.001$	$0.005 \pm 0.002 \pm 0.002$	$0.004 \pm 0.001 \pm 0.001$
−3.81	$0.005 \pm 0.001 \pm 0.001$	$0.007 \pm 0.002 \pm 0.002$	$0.006 \pm 0.001 \pm 0.001$
−3.68	$0.007 \pm 0.001 \pm 0.000$	$0.011 \pm 0.003 \pm 0.002$	$0.014 \pm 0.002 \pm 0.001$
−3.56	$0.014 \pm 0.001 \pm 0.002$	$0.019 \pm 0.004 \pm 0.004$	$0.027 \pm 0.003 \pm 0.002$
−3.43	$0.027 \pm 0.001 \pm 0.003$	$0.032 \pm 0.005 \pm 0.005$	$0.055 \pm 0.004 \pm 0.003$
−3.31	$0.054 \pm 0.002 \pm 0.004$	$0.068 \pm 0.007 \pm 0.006$	$0.105 \pm 0.005 \pm 0.007$
−3.18	$0.100 \pm 0.002 \pm 0.006$	$0.118 \pm 0.009 \pm 0.015$	$0.181 \pm 0.006 \pm 0.006$
−3.06	$0.171 \pm 0.003 \pm 0.004$	$0.191 \pm 0.011 \pm 0.008$	$0.265 \pm 0.007 \pm 0.006$
−2.93	$0.254 \pm 0.003 \pm 0.011$	$0.267 \pm 0.012 \pm 0.013$	$0.323 \pm 0.008 \pm 0.014$
−2.81	$0.316 \pm 0.004 \pm 0.011$	$0.325 \pm 0.013 \pm 0.018$	$0.335 \pm 0.008 \pm 0.007$
−2.68	$0.344 \pm 0.004 \pm 0.004$	$0.328 \pm 0.013 \pm 0.013$	$0.308 \pm 0.008 \pm 0.006$
−2.56	$0.331 \pm 0.004 \pm 0.004$	$0.297 \pm 0.013 \pm 0.013$	$0.270 \pm 0.007 \pm 0.006$
−2.43	$0.289 \pm 0.003 \pm 0.009$	$0.253 \pm 0.012 \pm 0.014$	$0.210 \pm 0.007 \pm 0.005$
−2.31	$0.231 \pm 0.003 \pm 0.006$	$0.196 \pm 0.011 \pm 0.005$	$0.161 \pm 0.006 \pm 0.005$
−2.18	$0.168 \pm 0.003 \pm 0.003$	$0.150 \pm 0.010 \pm 0.009$	$0.113 \pm 0.005 \pm 0.005$
−2.06	$0.113 \pm 0.002 \pm 0.003$	$0.117 \pm 0.009 \pm 0.006$	$0.080 \pm 0.004 \pm 0.002$
−1.93	$0.074 \pm 0.002 \pm 0.002$	$0.089 \pm 0.008 \pm 0.006$	$0.052 \pm 0.004 \pm 0.003$
−1.80	$0.044 \pm 0.002 \pm 0.002$	$0.058 \pm 0.006 \pm 0.007$	$0.030 \pm 0.003 \pm 0.003$
−1.68	$0.025 \pm 0.001 \pm 0.002$	$0.035 \pm 0.005 \pm 0.004$	$0.018 \pm 0.002 \pm 0.003$
−1.55	$0.012 \pm 0.001 \pm 0.001$	$0.018 \pm 0.004 \pm 0.002$	$0.009 \pm 0.002 \pm 0.002$
−1.43	$0.007 \pm 0.001 \pm 0.001$	$0.008 \pm 0.003 \pm 0.002$	$0.005 \pm 0.001 \pm 0.001$
−1.30	$0.004 \pm 0.001 \pm 0.001$	$0.003 \pm 0.001 \pm 0.004$	$0.001 \pm 0.001 \pm 0.001$
−1.18		$0.001 \pm 0.001 \pm 0.001$	$0.001 \pm 0.000 \pm 0.000$

0.06 for 38.3 GeV and 0.21 for 44 GeV. The results at each energy point are shown in Fig. 3 and compared with the predicted running of α_S based on QCD and on the world average value of $\alpha_S(M_{Z^0})$. For clarity the values at 34.6 and 35 GeV have been combined at their luminosity weighted average energy $\sqrt{s} = 34.8$ GeV using the combination procedure described above. The combined value is $\alpha_S(34.8\,\text{GeV}) = 0.1368 \pm 0.0005(\text{stat.}) \pm 0.0017(\text{exp.}) \pm 0.0032(\text{had.}) \pm 0.0011(\text{theo.})$. The results of ALEPH [10], DELPHI [11] and OPAL [12] are shown as well.

5.3 Renormalization scale dependence of α_S

For the fits in Sect. 5.2 the renormalization scale factor is set to the natural choice $x_\mu = 1$, where the energy dependence of (3) comes only from the running of the coupling α_S. However, different schemes for the determination of the renormalization scale factor are proposed. As a cross check of our default result we investigate in this section two more choices of the renormalization scale factor.

In the optimized renormalization scheme [32] the minimization is performed for all energy points with α_S and x_μ treated as free parameters. The systematic uncertainties are determined using the optimized renormalization scale determined in the default fit. The value of α_S, the optimized scale $x_\mu^{\rm opt}$ and their correlation are summarized in Table 3. The variation of χ^2/d.o.f. as a function of the scale x_μ is shown in Fig. 4. The combination of all energy points at $\sqrt{s} \geq 22$ GeV using the method described in Sect. 5.2[5] yields

$$\alpha_S(M_{Z^0}) = 0.1161 \pm 0.0005(\text{stat.}) \pm 0.0012(\text{exp.}) \pm 0.0022(\text{had.}). \quad (8)$$

The values for $x_\mu^{\rm opt}$ for centre-of-mass energies of 14, 22, 34.6, 35 and 43.8 GeV are within their statistical uncertainties covered by the systematic variation ($0.5 < x_\mu < 2.0$) of the default fit.

The second choice for the determination of the renormalization scale factor followed approximately the approach of "minimal sensitivity" (PMS) suggested by [33]. The renormalization scale factor $x_\mu^{\rm min}$ is specified by the point with α_S having the least sensitivity to the renormalization scale factor x_μ. The variation of α_S as a function of x_μ is shown in Fig. 4. The renormalization scale factor $x_\mu^{\rm min}$ is determined by a fit to the α_S variation with respect to

[5] In this case the statistical, experimental and hadronization uncertainty only contribute to the diagonal elements of the covariance matrix V'.

x_μ around the minimum. The determination of α_S is then repeated with x_μ set to $x_\mu^{\min}$. At 14 GeV the variation of α_S with respect to the renormalization scale factor has no minimum and therefore no fit is performed. The renormalization scale factor $x_\mu^{\min}$ as well as the result of the fit are summarized in Table 4. The systematic uncertainties are determined using $x_\mu^{\min}$ determined in the default fit.

The combination of all energy points above $\sqrt{s} \geq 22$ GeV using the method described in Sect. 5.2[5] yields

$$\alpha_S(M_{Z^0}) = 0.1155 \pm 0.0004(\text{stat.}) \pm 0.0012(\text{exp.}) \pm 0.0022(\text{had.}), \quad (9)$$

consistent with (7). The local minimum of α_S as a function of x_μ, is very close the natural scale $x_\mu = 1$ leading to a fitted value of α_S similar to the default value (7).

The choice of the renormalization scale factor $x_\mu^{\min}$ and x_μ^{opt} returns a value of α_S which is within the variation of the systematic uncertainty due to missing higher order terms. We therefore conclude that the evaluation of theoretical uncertainties using the commonly used standard method of setting x_μ to 0.5 and 2. safely includes alternative methods of the choice of the renormalization scale factor.

6 Summary

In this paper we present measurements of the strong coupling from the four-jet rate at centre-of-mass energies between 14 and 44 GeV using data of the JADE experiment. The predictions of the PYTHIA, HERWIG and ARIADNE Monte Carlo models tuned by OPAL to LEP 1 data are found to be in agreement with the measured distributions.

From a fit of QCD NLO predictions combined with resummed NLLA calculations with x_μ=1 to the four-jet rate corrected for experimental and hadronization effects we have determined the strong coupling α_S. In addition we investigated two more choices for the determination of the renormalization scale and found the results to be consistent. The value of $\alpha_S(M_{Z^0})$ is determined to be $\alpha_S(M_{Z^0}) = 0.1159 \pm 0.0028$ (total error). The natural choice of the renormalization scale $x_\mu = 1$ is close to the renormalization scale factor with α_S having the least sensitivity to the renormalization scale factor, $\frac{d\alpha_S}{dx_\mu} = 0$. Therefore the theoretical uncertainty determined by setting the scale x_μ to x_μ=0.5 and x_μ=2.0 yields smaller theoretical uncertainties than e.g. for fits to event shape observables [16]. This is also true for measurements of α_S performed at LEP energies [12].

References

1. B. Naroska, Phys. Rep. **148**, 67 (1987)
2. S. Catani et al., Phys. Lett. B **269**, 432 (1991)
3. L.J. Dixon, A. Signer, Phys. Rev. D **56**, 4031 (1997)
4. Z. Nagy, Z. Trocsanyi, Phys. Rev. D **57**, 5792 (1998)
5. Z. Nagy, Z. Trocsanyi, Phys. Rev. D **59**, 014020 (1998); Erratum, ibid. **62**, 099902 (2000)
6. JADE Collaboration, W. Bartel et al., Phys. Lett. B **115**, 338 (1982)
7. JADE Collaboration, W. Bartel et al., Z. Phys. C **33**, 23 (1986)
8. JADE Collaboration, S. Bethke et al., Phys. Lett. B **213**, 235 (1988)
9. JADE and OPAL Collaboration, P. Pfeifenschneider et al., Eur. Phys. J. C **17**, 19 (2000)
10. ALEPH Collaboration, A. Heister et al., Eur. Phys. J. C **27**, 1 (2003)
11. DELPHI Collaboration, J. Abdallah et al., Eur. Phys. J. C **38**, 413 (2005)
12. OPAL Collaboration, G. Abbiendi et al., Eur. Phys. J. C **47**, 295 (2006)
13. OPAL Collaboration, G. Abbiendi et al., Eur. Phys. J. C **20**, 601 (2001)
14. JADE Collaboration, P.A. Movilla Fernández et al., Eur. Phys. J. C **1**, 461 (1998)
15. P.A. Movilla Fernández, In: ICHEP 2002, Proceedings of the 31st International Conference on High Energy Physics, Elsevier Science B.V.
16. P.A. Movilla Fernández, Studien zur Quantenchromodynamik und Messung der starken Kopplungskonstante α_S bei $\sqrt{s} = 14$–44 GeVmit dem JADE-Detektor, Ph.D. thesis, RWTH Aachen, (2003) PITHA 03/01
17. T. Sjöstrand, Comput. Phys. Commun. **82**, 74 (1994)
18. G. Marchesini et al., Comput. Phys. Commun. **67**, 465 (1992)
19. E. Elsen, Detector Monte Carlos, JADE Computer Note 54 (unpublished)
20. E. Elsen, Multihadronerzeugung in e^+e^- Vernichtung bei PETRA-Energien und Vergleich mit Aussagen der Quantenchromodynamic, Ph.D. thesis, Universität Hamburg (1981)
21. C. Bowdery, J. Olsson, The JADE SUPERVISOR Program, JADE Computer Note 73 (unpublished)
22. P.A. Movilla Fernández, A Guide to the Resurrected JADE Data and Software, JADE Computer Note 103 (unpublished)
23. L. Lönnblad, Comput. Phys. Commun. **71**, 15 (1992)
24. OPAL Collaboration, G. Alexander et al., Z. Phys. C **69**, 543 (1996)
25. OPAL Collaboration, G. Abbiendi et al., Eur. Phys. J. C **35**, 293 (2004)
26. JADE Collaboration, W. Bartel et al., Phys. Lett. B **88**, 171 (1979)
27. JADE Collaboration, W. Bartel et al., Phys. Lett. B **129**, 145 (1983)
28. S. Brandt et al., Phys. Lett. **12**, 57 (1964); D. Fahri et al., Phys. Rev. Lett. **39**, 1587 (1977)
29. S. Bethke, Nucl. Phys. Proc. Suppl. **135**, 345 (2004)
30. K.G. Hayes, M. Perl, B. Efron, Phys. Rev. D **39**, 274 (1989)
31. OPAL Collaboration, G. Abbiendi et al., Eur. Phys. J. C **40**, 287 (2005)
32. OPAL Collaboration, P.D. Acton et al., Z. Phys. C **55**, 1 (1992)
33. P.M. Stevenson, Phys. Rev. D **23**, 2916 (1981)